UNESCO Chair on
Coastal Geo-Hazard Analysis
Research Institute for Earth Sciences
Geological Survey of Iran

unesco Chair

Abstract:

The Makran Accretionary Prism (MAP) is one of the largest accretionary prisms in the world. It is the result of convergence, initiated during the Late Cretaceous, between the Arabian and Eurasian plates. The MAP has grown seawards by frontal accretion and underplating of trench-fill sediments since the Miocene. Today, the system is characterized by a shallow dipping slab (<2°), great sediment thickness (>7 km) in the foreland of the Oman Sea and a wedge width of >500 km, >300 km of which are exposed onshore. New mapping and structural sections document the stratigraphic and structural developments of the central Makran Accretionary Wedge (MAW) in southern Iran. Four main tectono-stratigraphic provinces were distinguished, which are from north to south: North-, Inner, Outer and Coastal Makran. North Makran is dominated by mafic to intermediate igneous rocks and tectonic mélanges in which igneous rocks and Cretaceous deep-water marine sediments are involved. Locally, Upper Cretaceous shallow-water limestone unconformably covers deformed Cretaceous sediments and igneous rocks. In addition, the first turbiditic sequences containing mafic fragments were deposited during the Late Cretaceous. To the south, above the Ghasr Ghand Thrust (Inner Makran), turbiditic deposition of sandstone and shale took place during the Early Eocene and Early Miocene with an upward thickening and shallowing trend. Younger sediments, Early–Middle Miocene, crop out mainly in Outer Makran, between the Ghasr Ghand and Chah Khan Thrusts.

ISBN: 978-622-5858-49-7

9 786225 858497

2023

UNESCO Chair on
Coastal Geo-Hazard Analysis
Research Institute for Earth Sciences
Geological Survey of Iran
unesco Chair

UNESCO Chair on
Coastal Geo-Hazard Analysis
Research Institute for Earth Sciences
Geological Survey of Iran
unesco Chair

Stratigraphy, Structural Geology and low-Temperature Thermochronology Across the Makran Accretionary Wedge in Iran

UCCGHA 010

2023

Stratigraphy, structural geology and low-temperature thermochronology across the Makran accretionary wedge in Iran

سرشناسه	دولتی، اصغر، ١٣٥٤- - Dolati, Asghar, 1975
عنوان و نام پدیدآور	Stratigraphy, structural geology and low-temperature thermochronology across the Makran accretionary wedge in Iran[Book]/ authors Asghar Dolati...[et al.]; employer Swiss Institute of Technology Zurich; supervisor Jean-Pierre Burg; with cooperation UNESCO Chair on Coastal Geo-Hazard Analysis; summarized Manouchehr Ghorashi.
مشخصات نشر	تهران: نشرخزه، ۱۴۰۲= ۲۰۲۳م.
مشخصات ظاهری	۷۲ص.: مصور؛ ۱۴ × ۲۱ س‌م.
شابک	978-622-5858-7-49
وضعیت فهرست نویسی	فیپا
یادداشت	زبان: انگلیسی.
یادداشت	عنوان به فارسی: چینه شناسی، زمین شناسی ساختاری و ترموکرونولوژی دمای پایین در سراسر گوه برافزایشی مکران در ایران.
یادداشت	authors Asghar Dolati, Daniel Bernoulli, Diane Seward, Eric Barrier.
یادداشت	کتابنامه:ص. ۵۶-۴۶.
موضوع	چینه‌شناسی -- ایران -- مکران
موضوع	Geology, Stratigraphic -- Iran -- Makran
موضوع	زمین‌شناسی -- ایران -- مکران
موضوع	Geology -- Iran -- Makran
شناسه افزوده	دولتی، اصغر، ۱۳۵۴-
شناسه افزوده	Dolati, Asghar, 1975-
شناسه افزوده	بورگ، ژان-پیر، ناظر
شناسه افزوده	Burg, J.-P. (Jean-Pierre)
شناسه افزوده	یونسکو. کرسی مخاطرات زمین شناختی ساحلی
شناسه افزوده	UNESCO Chair on Coastal Geo-Hazard Analysis
شناسه افزوده	موسسه فناوری زوریخ سوئیس
شناسه افزوده	Eidgenössische Technische Hochschule Zürich
رده بندی کنگره	QE۶۵۱
رده بندی دیویی	۷/۵۵۱
شماره کتابشناسی ملی	۹۳۶۹۶۳۰

Stratigraphy, structural geology and low-temperature thermochronology across the Makran accretionary wedge in Iran

Author: Asghar Dolati

نشرخزه

اطلاعات گزارش

عنوان: چینه شناسی، زمین شناسی ساختاری و ترموکرونولوژی دمای پایین در سراسر گوه برافزایشی مکران در ایران

مجری: موسسه فناوری سوئیس زوریخ

زبان مرجع: انگلیسی

خروجی: گزارش، نقشه، مقاله، داده های الکترونیکی، پایان نامه دکتری

ناظر علمی: ژان پیر بورگ

نویسندگان: اصغر دولتی، دنیل بِرنوولی، دِین سِوارد، اریک بَرییر

رئیس کرسی یونسکو در مخاطرات زمین شناختی ساحلی: حمید نظری

مسئول شورای اجرایی: راضیه لک

خلاصه‌نویسی: منوچهر قرشی

ناشر: نشر خزه

با همکاری کرسی یونسکو در مخاطرات زمین شناختی ساحلی

چاپ اول: ۱۴۰۲

شمارگان: ۵۰ نسخه

صفحات: ۷۲

شابک: ۹۷۸-۶۲۲-۵۸۵۸-۷-۴۹

khazepub@gmail.com

Report Information

Title: Stratigraphy, structural geology and low-temperature thermochronology across the Makran accretionary wedge in Iran

Employer: Swiss Institute of Technology Zurich

Original language: English

Output: Report, Map, Paper, Digital Meta Data, Thesis Ph.D.

Supervisor: Jean-Pierre Burg

Authors: Asghar Dolati, Daniel Bernoulli, Diane Seward, Eric Barrier

Chairholder in the UNESCO Chair on Coastal Geo-Hazard Analysis: Hamid Nazari

Head of the Executive Council: Razyeh Lak

Summarized: Manouchehr Ghorashi

Publisher: Khazeh Publication

with cooperation UNESCO Chair on Coastal Geo-Hazard Analysis

First Edition: 2023

Edition number: 50

Page: 72

Shabak: 978-622-5858-7-49

khazepub@gmail.com

Scientific Council

Name	Affiliation
Ara Avagyan	IGS: Institute Geological Sciences
Rick J Bailey	IOC-UNESCO Indian Ocean Tsunami Warning and Mitigation System/ UNESCO
Aram Fathian Baneh	University of Calgary
Wenjiao Xiao	Chinese Academy of Sciences
Philippe Agard	University of Sorbonne
Eric Barrier	University of Sorbonne
Justin Ahanhanzo	Intergovernmental Oceanographic Commission of UNESCO (IOC-UNESCO)
Alice Aurelie	UNESCO Water Sciences Division
Klaus Reicherter	Aachen University
Judith Thomalsky	German Archaeological Institute Tehran Branch
Martin Hanz	German under water archaeology association
Hamid Alizadeh Lahijani	Iranian National Institute for Oceanography and Atmospheric Science
Yahya Djamour	Shahid Beheshti University (SBU)
Hassan Fazeli Nashli	University of Tehran
Razyeh Lak	Research Institute for Earth Sciences
Mohammad Mokhtari	International Institute of Earthquake Engineering and Seismology
Hamid Nazari	Research Institute for Earth Sciences

Jafar Omrani	Geological Survey of Iran
Mohammad Tatar	International Institute of Earthquake Engineering and Seismology
Morteza Talebian	Research Institute for Earth Sciences
Mehdi Zare	International Institute of Earthquake Engineering and Seismology
Stefano Salvi	National Institute of Geophysics and Volcanology (INGV)
Ryo Anma	Tokushima University
John Lambert	Deltares, UNESCO
Issa El-Hussain	Sultan Qaboos University
Egor Krasinskiy	Underwater research center Russian Geographical Society
Richard Walker	University of Oxford
Audemard Franck A.	Department of Geology, Central University of Venezuela
Wenjiao Xiao	Chinese Academy of Sciences
Jean-François Ritz	University of Montpellier
Ekkehard Holzbecher	German University of Technology in Oman
Yeong Bae Seong	Korea University

Executive Committee

Name	Affiliation
Dr. Razyeh Lak	Head of RIES and Executive Manager
Mahmoudreza Majidifard	Research Institute for Earth Sciences
Manouchehr Ghorashi	Research Institute for Earth Sciences
Alireza Vaezi	Research Institute for Earth Sciences
Arash Amini	Golestan University

Mohammad Tatar	International Institute of Earthquake Engineering and Seismology
Mohammad reza Ghasemi	Research Institute for Earth Sciences
Jafar Hassanpour	University of Tehran
Ataollah Dadashpour	Geological Survey of Iran, Sari branch
Ahmadreza Rabani	University of Science and Technology of Mazandaran
Ahmad Rashidi	International Institute of Earthquake Engineering and Seismology
Masoud Sadri Nasab	University of Tehran
Hasan Fazelinashli	University of Tehran
Abdolazaim Ghanghormeh	Golestan University
Ataollah Kavian	Environmental Protection Organization of Mazandaran Province
Seyed Mohsen Mortazavi	Hormozgan University
Nasir Ahmadi	Environmental Protection Organization of Mazandaran Province
Hasan Nasrollah Zadeh Saravi	Caspian Sea Ecological Research Center
Mojtaba Yamani	University of Tehran
Ahmed Hadidi	German University of Technology in Oman (GUTECH)
Alireza Amrikazemi	Scientific Coordinator, Qeshm Island UNESCO Global Geopark
Mahdi Rahmanian	Shargh Daily newspaper
Mohammad Salamati	Respina Company
Mohammadreza Kazemzadeh	Superme Audit Gourt

Secretariat

Name	Affiliation
Elnaz Aghaali	Research Institute for Earth Sciences
Hamoon Memarian	Research Institute for Earth Sciences
Hourieh AliBeygi	Research Institute for Earth Sciences
Shirin Zarei	Research Institute for Earth Sciences
Keivan Ajdari	Research Institute for Earth Sciences
Sedigheh Ghanipour	Research Institute for Earth Sciences
Shirin Safavi	Research Institute for Earth Sciences
Leila Shirazi	Research Institute for Earth Sciences
Aazam Takhtchin	Research Institute for Earth Sciences
Hanieh Bakhshaei	Geological Survey of Iran
Reza Behbahani	Geological Survey of Iran
Javad Darvishi khatooni	Geological Survey of Iran
Mohammadreza Ensani	Geological Survey of Iran
Marziyeh Estrabi Ashtiyani	Geological Survey of Iran
Gholamreza Hoseinyar	Geological Survey of Iran
Mojtaba Kavianpour Sangno	Geological Survey of Iran
Mehrnoosh Pour Saeid	Graphic Designer

Contents

Table of Figures

Abstract

The Makran Accretionary Prism (MAP) is one of the largest accretionary prisms in the world. It is the result of convergence, initiated during the Late Cretaceous, between the Arabian and Eurasian plates. The MAP has grown seawards by frontal accretion and underplating of trench-fill sediments since the Miocene. Today, the system is characterized by a shallow dipping slab (<2°), great sediment thickness (>7 km) in the foreland of the Oman Sea and a wedge width of >500 km, >300 km of which are exposed onshore. New mapping and structural sections document the stratigraphic and structural developments of the central Makran Accretionary Wedge (MAW) in southern Iran. Four main tectono-stratigraphic provinces were distinguished, which are from north to south: North-, Inner, Outer and Coastal Makran. North Makran is dominated by mafic to intermediate igneous rocks and tectonic mélanges in which igneous rocks and Cretaceous deep-water marine sediments are involved. Locally, Upper Cretaceous shallow-water limestone unconformably covers deformed Cretaceous sediments and igneous rocks. In addition, the first turbiditic sequences containing mafic fragments were deposited during the Late Cretaceous. To the south, above the Ghasr Ghand Thrust (Inner Makran), turbiditic deposition of sandstone and shale took place during the Early Eocene and Early Miocene with an upward thickening and shallowing trend. Younger sediments,

Early–Middle Miocene, crop out mainly in Outer Makran, between the Ghasr Ghand and Chah Khan Thrusts. They consist of shallow-water carbonates with Burdigalian (ca. 20–17 Ma) sandstones and marls. Coastal Makran, to the south, represents a wedge-top basin with a shallowing-upwards sequence from slope marls to coastal and continental deposits. All the provinces, Coastal Makran excepted, are covered unconformably by a large olistostrome including giant blocks of igneous and sedimentary rocks from North Makran and of sediments from Inner Makran. This olistostrome was emplaced during the Tortonian (11.6–9.6 Ma). The main tectonic activity took place during the Early to Middle Miocene as documented by unconformities and growth structures. Shortening was accommodated by regional-scale E-W trending thrusts. The Outer and Coastal Makran are much less deformed than the inner region. The typical structures in this area are open synclines with long (>20 km) wavelength and low amplitude alternating with tighter anticlines. Recent normal faults are common in Coastal Makran. Low temperature thermochronology (apatite and zircon fission-track ages) provides new time constraints on the evolution of the MAW. All apatites of Late Cretaceous to Miocene age have undergone partial annealing (60º–110º) after sedimentation. This implies that these sediments were never buried to temperatures reaching the full closure of the apatite fission-track system. The presently outcropping sequences were exhumed above a major décollement, possibly along the

Upper Oligocene shales, at a depth of about 5–6 km. In agreement with the burial temperatures estimated from apatites, the zircon ages were nowhere reset and hence yield detrital grain ages. Combining the new stratigraphic data and the apatite fission-track ages, a general progression of deformation is revealed passing from north to south, from <23 Ma in North Makran to about 7.9 Ma in Outer Makran. Out of sequence thrusting is due to post-olistostrome reactivation of older thrusts.

Introduction:

General Background

The Makran is one of the largest accretionary wedges on Earth. Located in SE Iran and South Pakistan, it extends ca. 1000 km from the Strait of Hormuz in the west to near Karachi in the east. The width of the wedge is 300-350 km from the offshore front of deformation to the depressions of Jaz Murian in Iran and Mashkel in Pakistan. More than half of the wedge is exposed on land. The other half, the active, frontal one, is below sea level. The Makran Accretionary Wedge (MAW) is an excellent example to study the geology and structures of an active convergent plate boundary involving subduction of the oceanic lithosphere. The elevation of the east-west trending mountain range rises from the coast up to 1800m in the north, along the southern border of the Jaz Murian Depression (Figure 1), which is about 350 m a.s.l. in its central part. The vegetation and the human population of the area are mostly concentrated along the rivers and the coast.

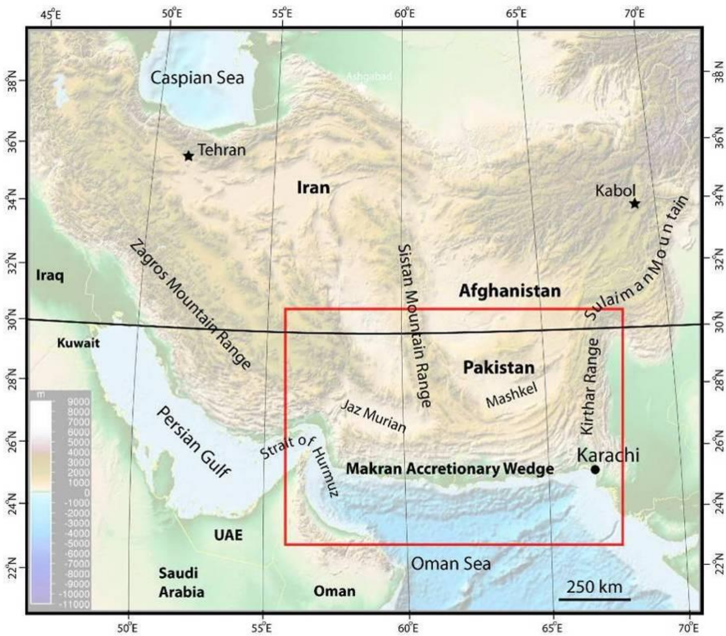

Figure 1: Geographic location of the Makran accretionary wedge in the frame of the surrounding mountain ranges. (background image, from ETOPO 5, http://www.ngdc.noaa.gov/mgg/global/etopo5.thml)

Geodynamic setting

Geodetic measurements indicate that the active convergence rate between Arabia and the Makran coast, measured between Mascat, in Oman, and Chabahar, on the Iranian Coast, is ca. 1.9 cm/year (Figure *2*). The present-day convergence rate between the Makran coast (Chabahar GPS) and stable Eurasia is ca. 8 mm/year (e.g. Vernant, et al. 2004) (Figure *2*).

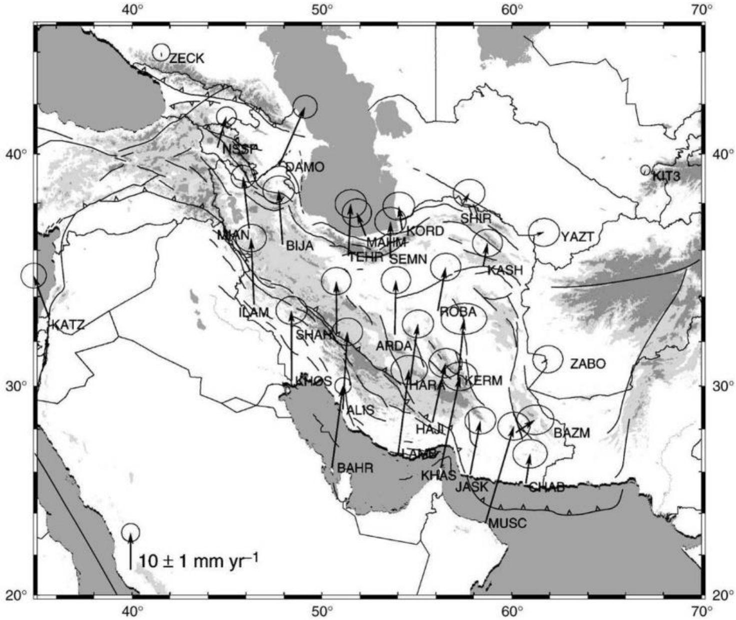

Figure 2: Horizontal velocity of the Middle East region superimposed on topography. The reference point is fixed in Eurasia (after Vernant et al. 2004).

The oceanic lithosphere of the Arabian plate is subducting northward under the Iranian Lut block and the Afghan/Helmand (also named Farah in old literature) Block (e.g. Stoneley 1974; Jacob and Quittmeyer 1979; McCall and Kidd 1982; Dercourt et al. 1986). The east–

west-trending Makran is located between two, nearly N–S transform fault systems. To the west, the dextral Minab Fault separates the Makran subduction zone from the Zagros continent–continent collision zone (e.g. Stöcklin 1968; Bird et al. 1975). To the east, the sinistral Chaman–Ornach–Nal fault system and its offshore continuation, the Owen fracture zone, separate Makran and the Arabian plate from the Indian continent (Figure *3*), which moves northward at 4–5 cm/a with respect to Eurasia (e.g. Paul et al. 2001 and Molnar 2009).

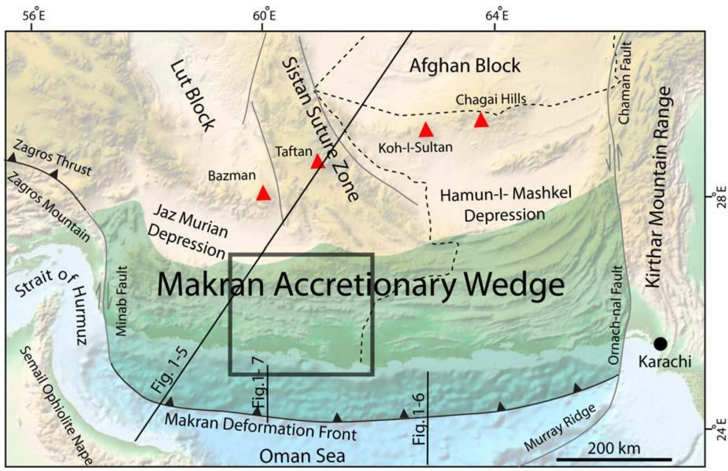

Figure 3: Tectonic setting of the Makran Accretionary wedge. Square: study area (background image, from ETOPO 5, http://www.ngdc.noaa.gov/mgg/global/etopo5.thml).

The magnetic anomalies of the Arabian oceanic crust in the Oman Sea are insufficiently clear to estimate its crustal age. Models of thermal cooling based on the mean surface heat flux of 42.6±3.6 mW m-2 suggest an age of 70–100 Ma (Hutchison et al. 1981). These authors noted that this age is consistent with the sediment-corrected basement depths of 5.5– 6.0 km and would place formation of the oceanic crust into the Cretaceous quiet zone.

The age of the Makran volcanic arcs (Bazman in Iran and Chagai Hills in Pakistan) suggests that subduction started in the Late Cretaceous (e.g. Arthurton et al. 1982; Berberian et al. 1982).

The Quaternary Baluchistan volcanic arc, which stretches from north of the Chagai Hills at the Pakistan/Afghanistan border into SE Iran, is associated with the ongoing Makran subduction zone (Figure *3* and Figure *4*). Three major volcanic centres, Bazman, Taftan and Kohi-Sultan form a ca. 300 km long belt (e.g. Jacob and Quittmeyer 1979; Berberian et al. 1982). The two large depressions to the south of Bazman and Koh-i-Soltan, Jaz Murian and Hamun-I-Mashkel, have been interpreted as forearc basins (Farhoudi and Karig 1977). The
relatively large, 400–600 km gap between the trench and the volcanic arc suggests that the subducting plate dips only 1-2º to the north (Figure *4*). Shallow subduction is consistent with seismic data (e.g. White and Klitgord 1976; White and Louden 1982) and earthquake focal mechanisms (e.g. Jacob and Quittmeyer 1979; Byrne et al. 1992; Engdahl et al. 2006; Alinaghi et al. 2007).

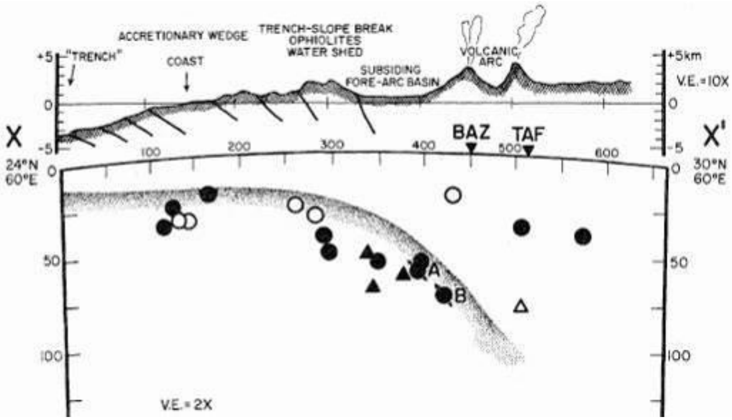

Figure 4: N–S section across Western Makran (60°E) after Jacob and Quittmeyer (1979). Lower shaded band = upper boundary of the descending oceanic lithosphere of the Arabian plate. The subduction slope increases below the Jaz Murian depression, interpreted as forearc basin. Circles represent events projected from up to 200 km to the east of the section line, triangles from up to 200 km to the west. Filled symbols = events for which depth is constrained by at least one depth phase; open symbols = events whose depth is determined by minimizing the residuals of first P arrivals. Tension axes (small arrows) of events A and B are calculated from focal mechanisms.

Seismic tomography images also a shallow slab below the Eurasian continent (Bijwaard et al. 1998 and Hafkenscheid et al. 2006) (Figure 5).

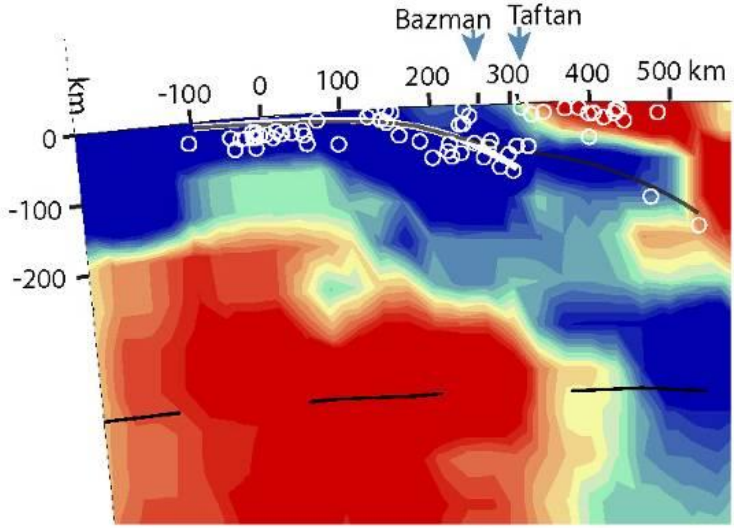

Figure 5: Interpolated tomography (background image, from Hafkenscheid et al. 2006) and earthquakes (white circles, after Engdahl et al. 2006) with subducting slab (thick white line drawn after Jacob and Quittmeyer 1979). Number -100 indicates the approximate location of the trench. Tomography section located Figure 3.

Seismic data across onshore Iranian Makran are not available but profiles across the coastal Pakistani Makran (e.g. Harms et al. 1984; Ellouz-Zimmermann et al. 2007) and the offshore Makran (e.g. White and Klitgord 1976; White and Louden 1982; Minshull et al. 1992; Kopp et al. 2000; Figure *6* and Figure *7*) are available. Wide angle seismic lines show an oceanic crustal thickness of ca. 9 km to the south of the trench (Fig. 1-6). The oceanic crust is covered by >7000 m of undeformed sediments at the front of the wedge. The total thickness of deformed and undeformed sediments reaches >10 km near the coast line (e.g. White and Louden 1982; Harms et al. 1984; Kopp et al. 2000; Fig. 1-6). Interpretation of wide-angle and reflection seismic data place a décollement at a depth of ca. 3-4 km near the deformation front (Figure 6). Sediments above the décollement are folded and thrust (e.g. White and Klitgord 1976; Harms et al. 1984 ; Grando and McClay 2006; Ellouz-Zimmermann et al. 2007; Figure 7). The sediments below the décollement move with the subducting oceanic crust (underplating of Platt, 1985) beyond at least the coast line (Kopp et al. 2000).

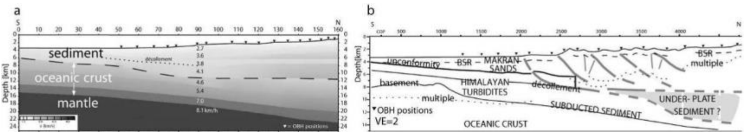

Figure 6: (a) Wide-angle seismic velocity model of offshore Makran (Kopp et al. 2000). Sediment thickness is 4-5 km in front of the Makran wedge and > 10 km near the coast line. Cross-section located in Figure 3. (b) Seismic interpretations across the wedge placing underplated sediments below a shallow dipping décollement.

The main accretion phase of the emerged wedge produced growth structures of Late Miocene to Early Pliocene age (Figure 7). Since the Late Pliocene, the coastal Makran and the mid-slope area have experienced surface uplift, normal faulting, shale extrusion and shortening (Harms et al. 1984; Grando and McClay 2006; Figure 7).

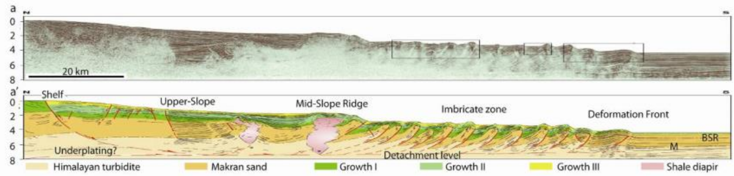

Figure 7: (a) N–S seismic profile across offshore Makran. In front of the prism, the M unconformity separates the fan deposits of Himalayan turbidites from the shelf–slope sediments of Makran sands. a´ = interpretation after Grando and McClay (2006) of seismic line in a, located in Figure 3.

The recorded seismicity in Makran is very low compared to the adjacent areas and most other subduction zones (Figure *8*). Byrne et al. (1992) suggest two seismically different segments. The western segment does not record any large historic event, nor has modern instrumentation detected any shallow event for the past 25 years: most earthquakes occur at about 70 km depth, within the down-going plate. In contrast to the west, earthquakes are common in the costal eastern segment and one large event (MW 8.1, November 1945) occurred at a depth of 30 km and propagated eastward along approximately 200 km of the length of the subduction zone (e.g. Page et al. 1979; Byrne et al. 1992 and Page et al 1979). Byrne et al. (1992) suggest segmentation of the subduction zone below central Makran where two seismic events showed dextral strike-slip motion (Figure *8*).

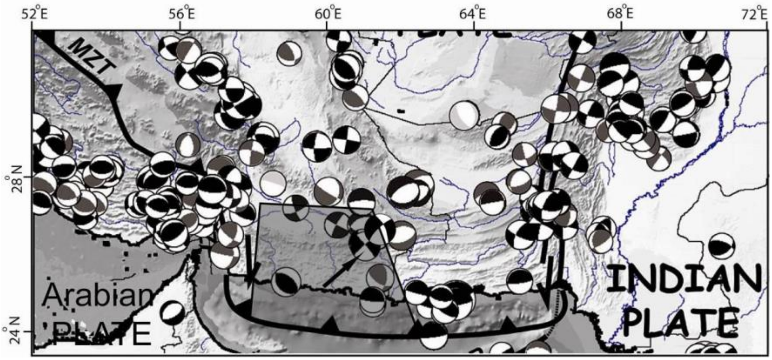

Figure 8: Major focal mechanisms over the MAW and adjacent areas. Hypocenters in 4 depth intervals: 0–30 km (black shaded); 30–60 km (dark grey shaded); 60–100 km (light grey shaded); and >100 km (very light grey shaded) compressive quadrants. Two dextral strike-slip events (arrowed) occurred on the boundary between the western (shaded) and eastern (non-shaded) segments. Data compiled from Quittmeyer and Kafka 1984; Laane and Chen 1989; Jacob and Quittmeyer 1979; Byrne et al.1992 and the Harvard CMT database.

A temperature gradient of about 20ºC km-1 was measured in wells in the onshore Pakistani Makran (Harms et al. 1984; Khan et al. 1991).

Motivation of this thesis and methods employed

The main goal of this project was to study the rheology of the accretionary wedge, especially the deformation behaviour of fluid saturated, porous rocks, and to investigate the interaction between deformation of the lithosphere and erosion and deposition on the surface. As discussed by Platt and Sathyendranath (1988), theories on the internal dynamics of wedges need to be confronted with observation, but actual tests are lacking because most active examples are submerged and ancient wedges have been affected by later tectonics. Most of the recent accretionary wedges (Barbados, Costa Rica, Nankai, Western Mediterranean) are submarine.

Their large-scale characteristics are interpreted from seismic profiles (e.g. Westbrook et al. 1988; Fruehn et al. 2002) and many sand-box experiments have simulated their bulk behaviour and growth (e.g. Westbrook et al. 1988; Schott and Koyi 2001; Kukowski et al. 2002). This study examines the on-shore MAW, which escaped collision. Excellent exposures allow placing any particular structure in its geological and regional context, which is difficult in submarine or less well exposed wedges like Taiwan. One aim was to evaluate the past and current deformation rates and total shortening associated with passed and active faulting, folding and penetrative deformation. We were particularly interested with two parameters of the dynamic equilibrium: 1) the internal deformation/rheology and 2) deformation/erosion coupling. Results were used to evaluate the variability and shifts in the style (compression versus extension) and location of deformation. Additionally, and key to this thesis, the project was also to produce a modern transect across the Makran to understand its role among the Tethys suture zones. First reconnaissance surveys have revealed that previous geological maps are less reliable than we expected. Consequently, basic fieldwork including the re-evaluation of stratigraphic ages and standard structural geology were necessary. The main objectives of this work are therefore (1) field geological studies and mapping to understand the internal deformation and stratigraphy of the inland Makran wedge and (2) low-temperature thermochronology to add a time framework to the studied structures and to quantify exhumation rates and erosion-denudation.

Geology

The main field studies were performed and geological maps of the MAW published more than 30 years ago. More recent studies are based on these previous geological maps, which were found to include important stratigraphic and structural errors. We surveyed detailed sections with systematic sampling for stratigraphy, geochronology and thermochronology purposes in order to draw a new geological map of the central part of the on-shore MAW. Field data, digital elevation models, analysis of multi spectral satellite images, biostratigraphic information and radiometric dating (U/Pb) on ash layers yielded significant information forcing to change fundamentally the existing maps.

Four main structural units with different lithostratigraphic and deformation histories are separated by major thrust zones (Figure *9*):

- North Makran contains Lower–Upper Cretaceous deep-marine sediments and volcanic rocks, in part assembled in tectonic mélanges. Ultramafic rocks were attributed to a JurassicPaleocene ophiolitic complex (McCall 1982). North Makran is weakly deformed.

- Inner Makran: consists of siliciclastic Eocene to Upper Oligocene and Miocene turbidites. Usually upward-thickening and –coarsening of the sedimentary layers indicate progradation of submarine fans. Close-tight folds and faulting/thrusting developed during Miocene, N–S compression.

- Outer Makran exposes mostly Lower-Middle Miocene sediments including sandstones, marls and locally shallow-water limestones. Open and large folds with a weak axial plane cleavage indicate lesser shortening than in Inner Makran.

A widespread Tortonian olistostrome covered the three previous units.

- Coastal Makran comprises sediments younger than Late Miocene. They are typical of shelf deposition which persisted in places up to Pleistocene times. Coastal Makran is only weakly deformed but exposes normal faults not seen in other units.

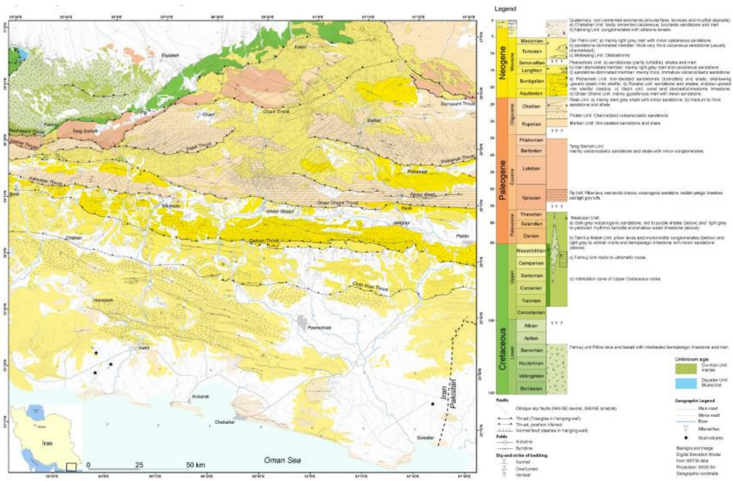

Figure 9: New geological map of the study area.

Coastal Makran

Coastal Makran forms the footwall of the Chah Khan Thrust Sheet and extends to the coast of the Gulf of Oman. Observed structures are essentially folds and faults.

Folds

Measurements and sections across Coastal Makran show open-gentle, rounded-blunt folds with very long wavelengths (>10 km) and low amplitudes (Figure *10*, Sections C to F). These folds are essentially symmetric, except south-vergent folds below the Chah Khan Thrust (Section B–C). Folds become relatively wider and more gentle southward (Figure *10*). Absence of axial plane cleavage and open folds indicate very weak deformation.

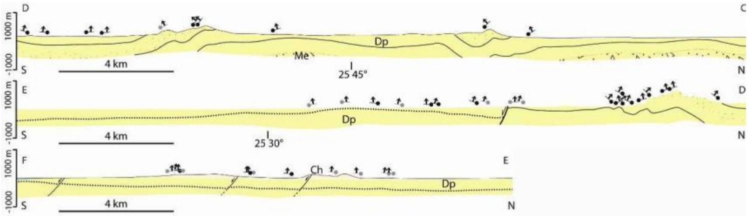

Figure 10: Sections across Coastal Makran; Dar Pahn (Dp), Metesang (Me) and Chabahar (Ch) Units. Folds are wider in the south. Measurements in grey were borrowed from the published geological maps of the area.

Fold axis measurements define nearly E–W folds exposed for several kilometres show fold axes plunging shallowly in either direction (Figure *11*). Layer measurements are consistent with the trends of the fold axes.

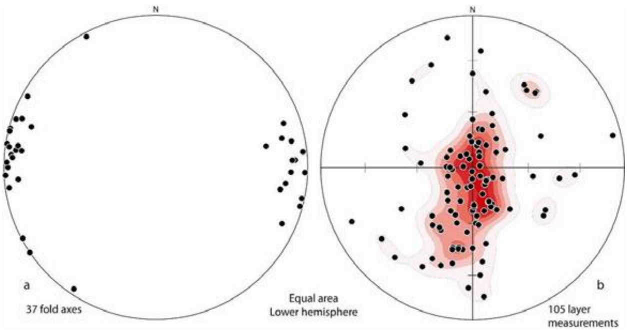

Figure 11: Fold axes (a) and layer measurements (poles) in Coastal Makran.

Paleostress regimes from brittle faults

Introduction

Several brittle fault zones were found in the studied part of MAW. The faults can be classified into three main populations (Appendix B): (1) Almost E–W striking thrusts; (2) NE–SW sinistral and NW–SE dextral strike slip faults; (3) nearly E–W striking normal faults occurring mostly near the coast. Paleostress tensors were calculated for all fault zones in order (1) to characterise the different sets and (2) to define the related stress tensors by inverse calculation.

Method

Many fault planes were measured throughout the mapped MAW. The shear sense was determined using classical kinematic indicators (e.g. Petit, 1987), such as the growth direction of mineral fibres, which usually are calcite. Isolated measurements were discarded, keeping 963 fault-slip data that represent 64 sites (*Figure 12* and *Table 1*). These fault sites are mainly located in major thrust zones, usually within uniform lithologies; they are usually observed over less than 200 m (at two sites over more than 200 m) but over a distance sufficient to ensure a reliable kinematic analysis. Each site comprises ten to twenty fault data with orientations measured to be varying as much as possible. The rake is according to the slip direction of the hanging wall with respect to the foot wall. It is measured from the strike direction and is positive counter clockwise (e.g. sinistral movement has a rake value of 180º, normal -90º and reverse +90º).

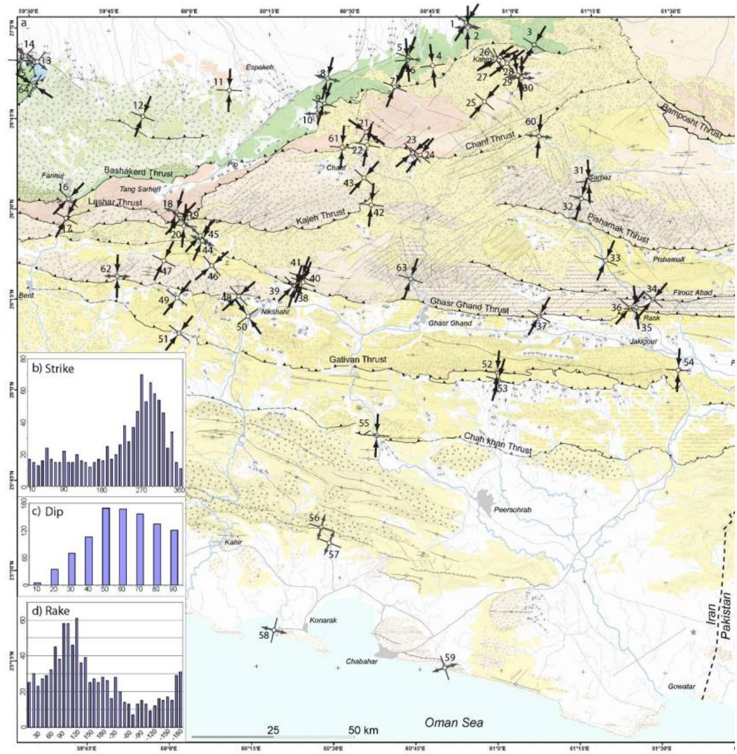

Figure 12: a) Principal stress axes projected onto the Figure 9 geological map. Locations (numbers) are given in Table 1. Inward and outward pointing arrows are maximum and minimum principal stress directions, respectively. Bars indicate the intermediate principal stress direction. Strike, dip and rake (b, c and d) defined in the text for the 963 fault data from the 64 locations.

The principal stress directions, S 1 (longest, compression), S 2 (intermediate) and S 3 (smallest, extension) were first approximated from bisecting and intersection directions of conjugate faults found in the field. This quick and simple estimate helped controlling the computer results. Paleostress inversion methods (e.g. Angelier, 1984; Etchecopar and Malavieille 1984, Burg et al. 2005) rely on the assumption that shear stress is parallel to the slip direction (Wallace, 1956; Bott, 1959), which is in turn given by fault striations. This assumption is acceptable, except when faults closely interact (Angelier, 1994; Dupin et al. 1993). Inversion methods seek principal stress directions, S 1, S 2 and S 3 with the S 1 direction as close as possible to that of the measured slicken lines (Appendix C) and calculate magnitude ratios r0= $(\sigma1-\sigma2)/(\sigma1-\sigma3)$ characterizing the shape of the stress ellipsoid. This approach is very successful in regions where finite strain is moderate because the requirement that a homogeneous state of stress has activated a significant subgroup of data is more likely to hold in such situations. In regions where the total strain is large, as in North and Inner Makran, a global analysis probably exceeds the limits of the method. However, faulting and folding typify deformation localized in space and time since these faults and folds are diachronous mechanical instabilities (e.g.; Cowie and Scholz, 1992). Therefore, separate sites may reflect juxtaposed episodes of moderate deformation for which the analytical method remains valid. Then, each result should be a reasonable solution documenting a local and temporal stage or state of stress.

Data processing was carried out with the Fault Slip Analysis (FSA) software of Célérier (1999). An effective stress tensor, with principal orientations S 1, S 2 and S 3 was separately calculated for each locality. This tensor, selected by random search trying 5000 tensors, had to accept an angular error smaller than 30º for 60% of the local fault-slip data. Any tensor obtained from less than 5 fault data was rejected. The 64 sites are those that yielded single tensors compatible with an adequate proportion of data. Data and geographic information about each site are listed in Table *1*.

Table 1: Fault sites from the studied MAW. Lab, label of site; az, Azimuth; pl, plunge; Mahaz, maximum horizontal stress axis; SV vertical stress axis; n, number of measured fault data; Exp, number of selected faults with angular error smaller than 30º from the calculated stress tensor; Str. stratigraphic age; Cr. Cretaceous; Eo. Eocene; Ol. Oligocene; E.M. Early Miocene; M.M. Middle Miocene; L.M. Late Miocene.

6	60° 40′ 52.8″	26° 56′ 20.3″	176	0.26	265.6	-55	266.2	35	0.88	355	3	8	6	Cr.
7	60° 38′ 55.6″	26° 52′ 00.1″	202	0.43	291.5	-37	292.3	52.8	0.66	202	3	10	6	Cr.
8	60° 26′ 0.6″	26° 53′ 1.62″	193	25.1	211.8	-64	286.9	7.23	0.67	14	2	18	10	Cr.
9	60° 25′ 29.3	26° 48′ 55.4″	192	21.7	294.5	29	70.6	52.4	0.69	198	3	20	9	Cr.
10	60° 24′ 16.6″	26° 47′ 6.78″	221	52.1	350.5	26.4	93.92	25.1	0.44	357	1	20	9	Cr.
11	60° 07′ 43.6″	26° 50′ 38.0″	181	15	272.3	6.05	23.7	73.8	0.63	182	3	10	1	Cr.
12	59° 51′ 47.3″	26° 46′ 01.2″	20.2	10.8	112.2	10.1	244.4	75.1	0.55	201	3	9	6	Cr.
13	59° 31′ 55.1″	26° 54′ 33.5″	115	83.5	219.5	1.6	309.7	6.31	0.57	219	1	15	9	Cr.
14	59° 29′ 37.6″	26° 55′ 30.3″	290	74.17	47.8	7.53	139.68	13.84	0.69	45	1	15	9	Cr.
15	59° 29′ 46.8″	26° 54′ 42.9″	56	87.15	92.85	-2.28	182.79	1.7	0.34	93	1	16	9	Cr.
16	59° 38′ 20.6″	26° 32′ 6.36″	44.1	1.23	134.9	33.5	312.2	56.4	0.31	224	3	14	8	Cr.
17	59° 38′ 18.8″	26° 28′ 50.4″	210	5.79	296	-31	309	58.3	0.66	28	3	11	8	Eo.
18	59° 58′ 23.2″	26° 30′ 6.72″	19.8	13.1	133.4	59.9	283.2	26.6	0.38	17	2	11	8	Eo.
19	59° 59′ 10.9″	26° 29′ 4.44″	219	33.1	246.4	-54	317.9	13.1	0.83	43	2	13	3	Eo.
20	59° 59′ 41.6″	26° 28′ 3.78″	186	10.8	273.8	-9	324.9	75.8	0.78	185	3	13	9	L.M
21	60° 33′ 26.2″	26° 44′ 09.4″	311	25.3	25.79	-29	75.16	50.1	0.33	304	3	11	9	Eo.
22	60° 33′ 37.6″	26° 42′ 06.1″	191	0.24	281.6	33.2	101.1	56.8	0.41	191	3	11	9	L.M
23	60° 42′ 03.7″	26° 40′ 52.5″	229	2.55	319.7	13.5	128.6	76.3	0.59	230	3	9	7	Eo.
24	60° 43′ 13.0″	26° 40′ 32.6″	220	31.6	306.2	-6.2	26.27	57.6	0.50	218	3	9	7	Eo.
25	60° 55′ 23.9″	26° 49′ 41.0″	41	0.25	131.1	24.5	310.4	65.4	0.75	221	3	10	6	Ol.
26	60° 57′ 14.3″	26° 56′ 48.4″	55.8	11.3	144.4	-6.7	204.2	76.8	0.74	235	3	16	9	Eo.
27	60° 57′ 40.9″	26° 56′ 43.4″	57.8	23.4	161.5	28.7	294.8	51.4	0.87	244	3	14	9	Eo.
28	60° 59′ 13.2″	26° 56′ 6.42″	38.2	9.06	138.9	49.4	300.7	39.2	0.84	223	3	14	10	Eo.
29	61° 01′ 35.2″	26° 54′ 2.88″	348	14.7	5.71	-75	79.63	4.34	0.14	349	2	11	6	Ol.
30	61° 01′ 41.5″	26° 53′ 43.0″	357	20.2	39.8	-64	93.54	16.4	0.77	180	2	13	7	Ol.
31	61° 14′ 38.6″	26° 36′ 28.3″	357	5.6	87.53	0.81	185.7	84.3	0.32	177	3	11	8	Ol.
32	61° 13′ 25.4″	26° 33′ 37.0″	14	19.2	104.8	2.3	201.4	70.7	0.56	15	3	11	7	Ol.
33	61° 18′ 02.9″	26° 23′ 25.8″	22.8	15.5	113.6	2.5	212.4	74.3	0.31	22	3	7	5	M.M.
34	61° 26′ 58.9″	26° 16′ 59.0″	221	5.97	309.5	-17	329.6	71.5	0.78	40	3	11	5	Ol.
35	61° 23′ 44.3″	26° 15′ 46.2″	349	23.4	87.01	17.9	210.8	59.8	0.93	173	3	15	9	Ol.
36	61° 23′ 03.3″	26° 15′ 40.0″	220	18.2	311.1	3.45	51.41	71.4	0.95	221	3	14	7	Ol.
37	61° 05′ 51.9″	26° 13′ 58.0″	27.4	22.7	120.2	6.75	225.8	66.2	0.75	209	3	12	7	Ol.
38	60° 20′ 47.5″	26° 18′ 26.1″	200	17.3	283.6	-18	330	64.3	0.85	197	3	15	9	Ol.
39	60° 20′ 22.4″	26° 18′ 31.9″	51.4	30.4	127.9	-22	188.4	51.2	0.49	224	3	12	8	Ol.
40	60° 21′ 58.8″	26° 19′ 06.9″	23.3	21.9	107.9	-13	169.2	64.1	0.81	201	3	14	9	Ol.
41	60° 21′ 46.0″	26° 19′ 36.1″	23.3	21.9	107.9	-13	169.2	64.1	0.81	201	3	11	9	Ol.
42	60° 34′ 27.8″	26° 32′ 03.8″	185	13	277.9	11.5	48.16	72.6	0.56	186	3	11	9	L.M.
43	60° 33′ 4.62″	26° 36′ 34.7″	207	39.6	321.9	27.1	75.85	38.5	0.34	221	3	11	7	Ol.
44	60° 03′ 22.6″	26° 25′ 39.4″	18.1	21.6	72.75	-56	118.9	25.4	0.43	24	2	15	10	L.M.
45	60° 02′ 55.9″	26° 26′ 17.6″	38.2	20.2	87.3	-61	136.1	20.3	0.98	222	2	9	6	L.M.
46	60° 05′ 9.6″	26° 21′ 20.6″	36.4	34.8	152.3	32.1	272.5	38.8	0.67	49	3	11	6	L.M.
47	59° 56′ 13.7″	26° 22′ 07.5″	23.4	7.56	117.2	26.2	278.6	62.5	0.58	26	3	12	11	Ol.
48	60° 10′ 19.8″	26° 16′ 25.0″	225	6.68	325.1	57.4	130.4	31.8	0.82	228	3	10	5	Ol.
49	59° 58′ 56.1″	26° 15′ 59.8″	38.4	43.6	126.9	-1.5	215.3	46.3	0.91	218	3	11	7	E.M.
50	60° 12′ 10.1″	26° 13′ 04.4″	326	10.9	50.13	-29	74.73	58.7	0.71	143	3	14	8	E.M.
51	59° 59′ 28.4″	26° 10′ 07.4″	34.5	32.1	132.4	12.4	240.7	55	0.62	218	3	10	7	E.M.
52	60° 58′ 22.4″	26° 04′ 31.7″	5.05	16.2	93.54	-5.2	166.2	73	0.83	185	3	21	17	M.M.
53	60° 58′ 22.7″	26° 03′ 27.5″	200	17.3	283.6	-18	330	64.3	0.85	196	3	8	6	M.M.
54	61° 31′ 52.7″	26° 05′ 28.5″	3.02	2.44	93.19	3.95	241.4	85.4	0.95	3	3	19	9	E.M.
55	60° 36′ 16.2″	25° 53′ 42.4″	3.02	2.44	93.19	3.95	241.4	85.4	0.95	3	3	12	8	M.M.
56	60° 26′ 27.9″	25° 38′ 23.2″	110.8	78.53	286.8	11.44	16.98	0.78	0.54	285	1	6	6	L.M.
57	60° 28′ 02.6″	25° 32′ 51.7″	164	77.1	291.9	8.09	23.35	10	0.75	112	1	9	7	L.M.
58	60° 18′ 10.0″	25° 21′ 11.4″	0.66	79.3	13.6	-10	103.2	2.33	0.72	14	1	5	4	L.M.
59	60° 40′ 30.8″	25° 15′ 27.5″	67.8	57	161.3	2.27	252.79	32.91	0.66	161	1	5	4	L.M.
60	61° 05′ 34.1″	26° 44′ 04.3″	8.36	20.43	145.2	62.96	271.86	16.93	0.83	5	2	6	5	L.M.

Results

Most of the maximum principal stress directions (S 1) plunge shallowly towards NNE or SSW (Figure *13 a*). This nearly horizontal compression is consistent with fold orientations, which suggests that folds and faults formed in the same stress field. Eight sites yielded vertical to subvertical maximum principal stress (Figure *13 a & b*), defining extension.

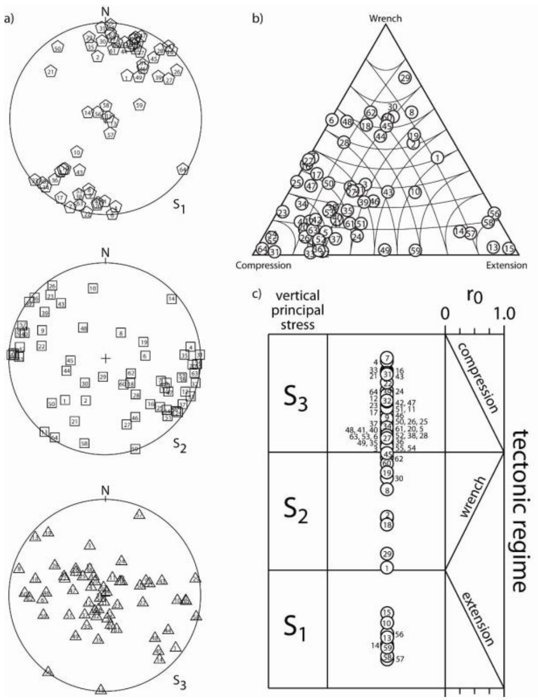

Figure 13: Plots of the 64 stress tensors of sites listed in Table 3-1. a) Equal area, lower-hemisphere projection of the principal stress axes S 1 , S 2 and S 3 . b) Triangular classification (Frohlich, 1992) of stress axes. c) Tectonic regime plot (Armijo et al. 1982; Philip, 1987; Célérier, 1995). S 1 , S 2 and S 3 are unit vectors with no magnitude; r0 =(σ1–σ2)/(σ1–σ3) where σi stands for principal stress magnitude.

The intermediate and minimum principal stress directions S 2 and S 3 scatter more than S 1. Stereoplots of principal stresses and the triangular diagram of Frohlich (1992) show few vertical principal stress directions (Figure *13 a & b*). This could be due to fold- or faultrelated rotation after the measured fault planes were activated by the calculated stress tensor. The tectonic regime plot (Figure *13 c*) confirms two faulting regimes: (1) compression to transpression and (2) extension.

The horizontal principal stress-direction map (Figure *12*) was produced by projecting two of the principal stress axes S 1, S 2 or S 3 onto the horizontal plane and so approximately fitting the Anderson assumption (Anderson, 1905), for which one stress axis is vertical.

Compression and transpression

Both compressional and transpressional regimes show subhorizontal to shallow plunging (<30º) S_1, in either NNE or SSW direction (Figure *14 a*). Stress components S_2 and S_3 are scattered on a subvertical plane perpendicular to S_1 (Figure *14 a*). Details for each site are presented in Appendix C. Site 40 and Site 8 are chosen to illustrate the compressional and transpressional tectonic regimes, respectively, because they are representative of a large number of fault data and document the quality of the results.

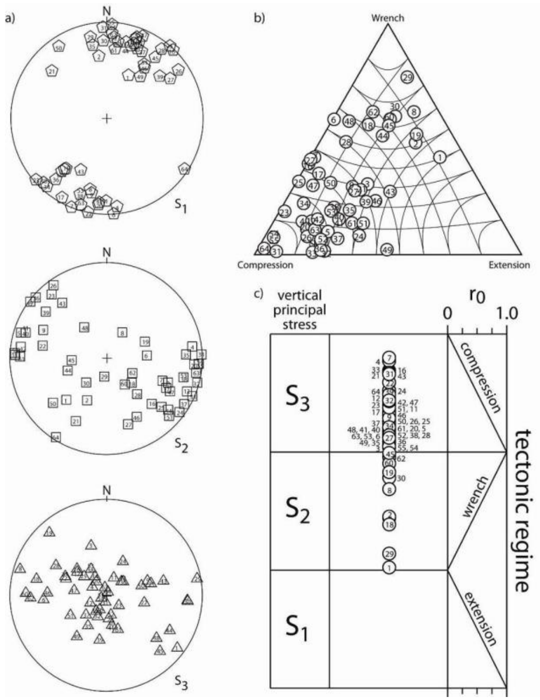

Figure 14: Plots of stress tensors for the compressional and transpressional regimes. Plot explanation in Figure 13. Data listed in Table 1.

- Compressional tectonic regime: Site 40

This site is in the direct hanging wall of the Ghasr Ghand Thrust, to the NE of Nikshahr. N- to NE-dipping reverse faults and conjugate S-dipping reverse faults are dominant (Figure *15 a*). Nine of fourteen measurements define the calculated paleostress tensor. This tensor has a NNW, subhorizontal maximum principal stress axis S 1 and a subvertical minimum stress axis S 3 (Figure *15 b*). S 1 is nearly perpendicular to the Ghasr Ghand Thrust zone (Figure *12*). A measure of how well the tensor explains the fault-slip data is given by the Mohr and angular error diagrams (Misfit) (Figure *15 c & d*). The stress state of each fault is plotted in the Mohr circle representing the calculated stress tensor, along with the friction lines S0. The slope of the friction line is defined by $S0=\mu/(\tau-\mu(\sigma nr-1))$, the required stress difference ratio to activate a fault plane. τ is shear stress and σnr the normal stress computed from the reduced stress tensor (considering a standard friction coefficient $\mu=0.6$, $S0 =(\sigma 1–\sigma 2)/\sigma 1)$. In these diagrams, one can see that the calculated stress tensor can activate 6 fault planes with a stress difference ratio $0.68\leq S0 \leq 0.8$ (Figure *15 c*). The Misfit angle plot (Figure *15 d*) shows that this tensor actually explains 9 faults with an angular error < 30º. The r0 value (0.81) indicates $\sigma 2$ being close to $\sigma 3$. This difficult identification explains scattering of the calculated S 2 and S 3 in the plane perpendicular to S 1. Thus, this site clearly records NNE–SSW compression.

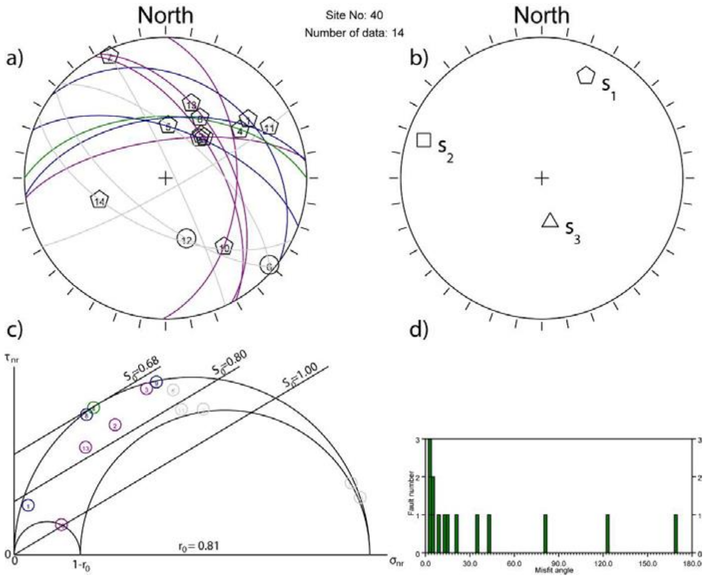

Figure 15: Fault and tensor data of Site 40 (location on Fig. 3-72). Stereographic, equal area lower hemisphere projections of a) fault-slip data (circles: normal slip and pentagons: reverse slip). b) Principal stress axes of the best tensor solution. c) Mohr-diagram (explanation in text). d) Misfit plot (explanation in text).

- Transpressional tectonic regime: Site 8

The site is located in the boundary zone between the Jaz Murian depression and the Imbricate Zone, east of Espakeh. Ten out of 18 fault-slip data are subvertical NE–SW sinistral strike slip faults (Figure *16 a*). The best-fit tensor obtained after inversion yields subhorizontal S 1 and S 3 shallowly plunging toward SSW and WNW, respectively, and a subvertical S 2 (Figure *16 b*). Ten faults have an angular error < 30º (Figure *16 d*). Nine of these ten faults can be activated by the calculated tensor with a stress difference ratio 0.68≤ S0 ≤0.8 (nine faults plot between the friction lines S0 =0.68 and S0= 0.8 in Figure *16 c*). This site reveals a wrench tectonic regime with well defined NNE–SSW-directed compression, hence transpression consistent with r0=0.68.

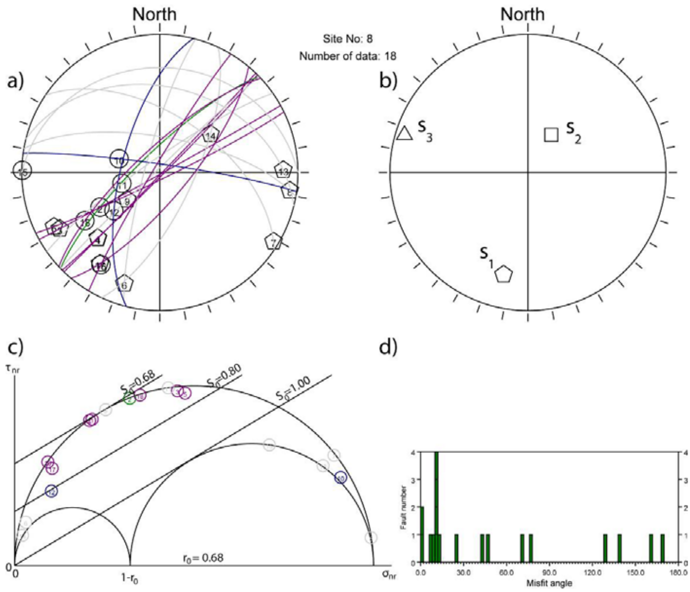

Figure 16: Fault and tensor projections for Site 8 (location Fig.3-72). Stereographic projections, Mohr-diagram and Misfit plot as in Figure 15. Data in Table 1.

Extension

Eight of the investigated sites yielded stress tensors with predominantly steep (>50º) stress components S_1 indicative of an extensional regime (Figure *17*). This regime is dominant in Coastal Makran and less obvious to the north of Fannuj, but again along the boundary of Jaz Murian (Figure *12*). Coastal Makran shows both E–W and N–S extension directions; the Jaz Murian boundary shows mostly N–S extension (Figure *12*). All details are given in Appendix C. The well constrained Site 15 is chosen to illustrate the extensional tectonic regime.

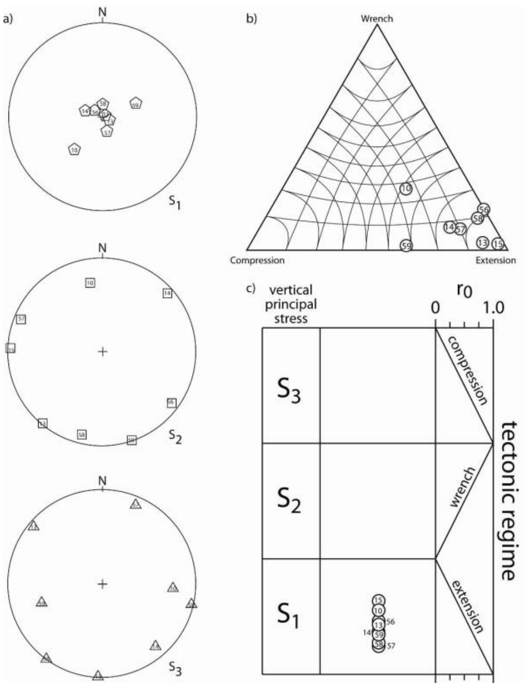

Figure 17: Extensional stress tensors. Plot explanations in Figure 13. Data in Table 1.

- Extensional tectonic regime: Site 15

This site of sixteen fault measurements (Figure *18 a*) is located in the contact zone between the Jaz Murian depression and the Imbricate Zone (Figure *12*). The best-fit tensor yields a vertical S 1 and subhorizontal S 2 and S 3 which plunge toward W and S, respectively (Figure *18 b*). The r0 value of 0.34 implies a well defined N–S extension direction.

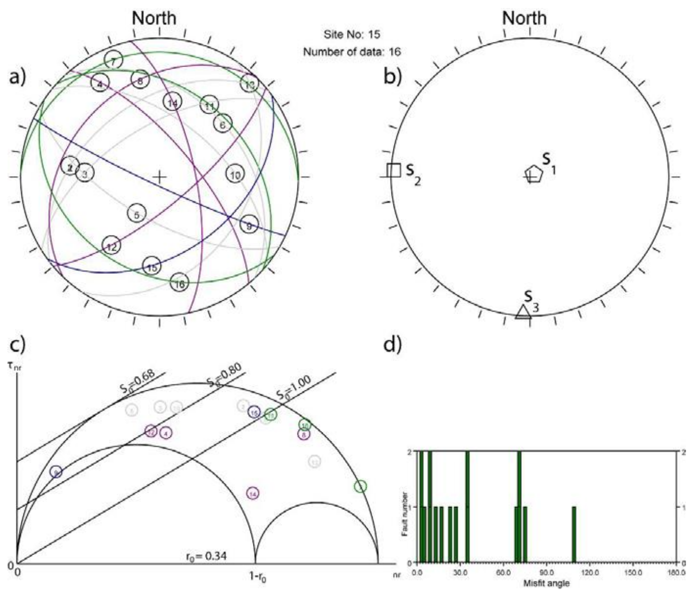

Figure 18: Extensional stress tensor at Site 15. Plot explanation in Figure 15.

Interpretation

The distribution and orientation of calculated paleostress tensors indicate regional NNE– SSW compression. This direction is consistent with mapped fold trends and major thrusts (Ghasr Ghand, Gativan, Pishamak and Lashar) as well as with the present-day convergence direction between the Arabian and Iranian plates (e.g. Nilforoushan et al. 2003; Reilinger et al. 2006). NE–SW compression is dominated in the north-northeastern part of the study area. Since it was obtained from faulted rocks older than Oligocene, this compression direction might represent an early event related to the N–S Sistan Suture Zone (Figure *3*), which is located next to the north of the study area. Paleostress calculations additionally substantiate the relative importance of wrenching besides thrusting in North Makran, especially in the Imbricate Zone and in northern Inner Makran (Figure *13*). r_0 values close to 1 (>0.80) for both compressional and wrench regimes suggest a flattened stress ellipsoid with subhorizontal σ_1. This ellipsoid shape may reflect shallow burial at the time of faulting.

Extension appears in two main areas:

Coastal Makran: The inland part contains well defined N–S extension with r_0 values of 0.5-0.6 that suggest prolate shapes of the stress ellipsoid with a vertical σ_1. Near the coast, extension is nearly E–W with rather large (0.66 - 0.73) r_0 values. Since σ_2 and σ_3 are almost equal, the sub-radial extension has a weakly defined direction. This tectonic regime is regional since normal faults also exist in the Pakistani Makran (e.g. Harms et al. 1984). Planar and bookshelf geometries with few meter displacements along individual faults indicate near surface faulting. However, seismic profiles exhibit large listric normal faults and planar small normal faults (e.g. Grando et al. 2007; Figure *19*). Some authors (e.g. Kopp et al. 2000; Grando et al. 2007) suggested that underplating caused uplift and extension in coastal and off-shore Makran.

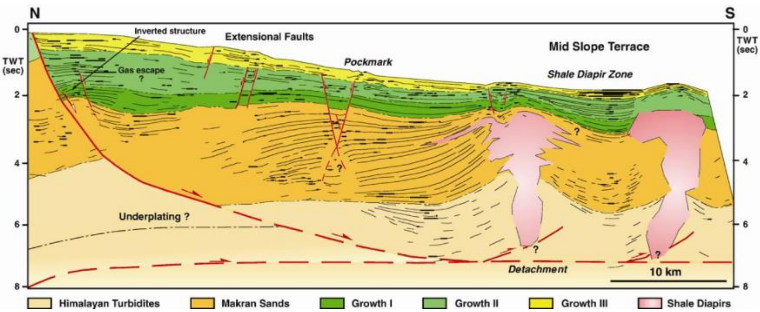

Figure 19: Normal listric fault on a seismic line in the Iranian off-shore Makran, near to the coast (Grando and McClay, 2006).

(2) North Makran yielded two extension directions, NW–SE to N–S and E–W. The site

with N–S extension has a small r0 value (0.34), which indicates that the extension direction is well constrained. Larger r0 (0.57 - 0.69) at other sites define weaker extension directions. We could not clarify the time-relation between N-S extension and compression there.

The area with E–W extension, to the east of Espakeh, is associated with a NE–SWtrending sinistral strike-slip fault. Where strike of the fault changes to almost N–S, the resulting fault geometry led to a local and small pull-apart basin. The subhorizontal S 3 plunging to the east could be a local effect in the releasing bend.

Recent stress field

Earthquake focal mechanisms were used to constrain the present-day stress field (Figure *20*). Twenty-eight focal mechanisms (Table *2* and Table *3*), scattered over and around the area, between longitude 58ºE and 64ºE and latitude 24ºN and 27ºN, were gathered from the literature and world-wide-web data bases (Byrne et al. 1992; Chandra 1984; Jackson and Mckenzie 1984; Quittmeyer and Kafka 1984 and Harvard CMT database).

Table 2: Earthquake focal mechanisms with defined P, B and T axes. az: azimuth and pl: plunge. Data from Harvard CMT database.

n	long (E)	Lat (N)	depth (km)	*mb*	Paz	Ppl	Baz	Bpl	Taz	Tpl	date
1	61.23	26.75	15	5.6	195	39	20	51	287	2	10.01.1979
2	61.31	26.75	15	5.6	184	36	22	52	280	9	10.01.1979
3	60.27	29.99	64	5.3	72	8	285	80	163	5	01.01.1980
4	58.86	25.59	15	5.7	43	8	311	8	177	78	07.12.1989
5	62.94	25.08	15	5.3	180	39	86	5	350	50	07.12.1991
6	62.88	24.25	15	5.6	177	36	83	6	345	53	30.01.1992
7	61.43	25.68	37	5.7	244	4	151	39	339	51	17.12.1992
8	60.91	27	72.4	5.3	89	73	259	17	350	3	24.06.2003

Table 3: Earthquake focal mechanisms with inferred fault plane, based on preferred orientation relative to local tectonics. References: Byr, Byrne et al. (1992); Ch, Chandra (1984); Qu, Quittmeyer and Kafka (1984); JM' Jackson and McKenzie (1984).

n	long (E)	Lat (N)	depth (km)	M_W	*mb*	Strike	Dip	Rake	date	References
1	63.48	26.15	27	7.9		246	7	89	27.11.1945	Byr
2	63.49	25.04	20	6.8		236	7	68	05.08.1947	Byr
3	60.95	26.55	3	5.8		256	61	13	10.01.1979	Byr
4	61.02	26.48	2	5.9		230	82	-4	10.01.1979	Byr
5	61.22	25.14	18	5.0		334	15	148	08.08.1972	Byr
6	62.87	25.19	26		4.7	290	49	-50	03.08.1968	Byr
7	62.75	24.99	18		5.1	279	9	84	13.02.1969	Byr
8	61.22	25.04	20		5.4	321	17	134	06.08.1972	Byr
9	61.22	25.14	18		5.4	334	15	148	08.08.1972	Byr
10	63.14	24.83	20		4.6	277	9	84	18.08.1972	Byr
11	63.21	24.88	18		5.2	281	23	70	02.09.1973	Byr
12	63.09	25.22	18		5.0	278	27	88	29.07.1975	Byr
13	62.40	25.33	18		5.1	214	16	19	10.02.1978	Byr
14	59.40	27.00	52		5.2	46	18	-90	29.05.1963	Ch
15	63.14	25.32	5		5.4	190	30	0	12.08.1963	Qu
16	61.22	25.04	33		5.5	292	22	114	06.08.1972	Ch
17	61.22	25.14	30		5.5	280	5	90	08.08.1972	Ch
18	63.21	24.88	30		5.3	270	30	90	02.09.1973	Qu
19	60.95	26.55	33		5.9	300	40	90	10.01.1979	JM
20	61.02	26.48	33		5.9	300	34	90	10.01.1979	JM

The P, B and T axes of focal mechanisms provide an acceptable indication of the active principal stress directions (Burg et al. 2005 and Célérier 1988) with P axes replicating S 1and T axes S 3 directions. In parallel, the tensor map of the area (Figure *21*) can be extracted from the calculated tensors (Table *1*) and compared with that of the earthquake focal mechanisms (Figure *20*).

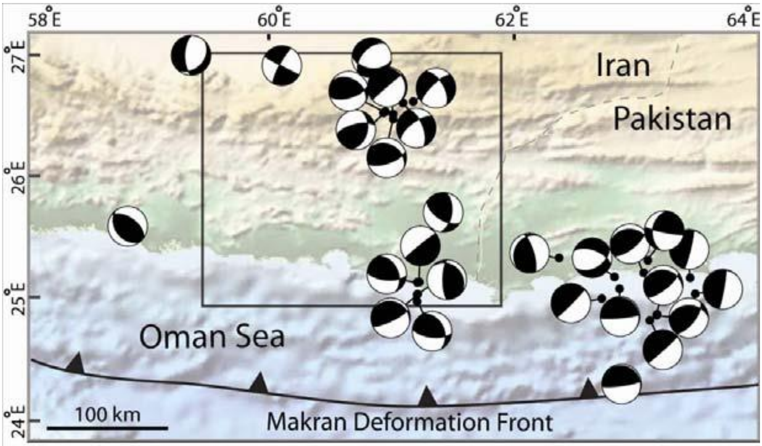

Figure 20: Focal mechanisms in central MAW. References and data in Table 2 and Table 3. Square = study area. Filled quadrants are compressional, empty quadrants are tensional.

Several focal mechanisms are located within the northern part of the studied area. They indicate nearly N–S compression, comparable with that obtained from the fault analysis. Similarly, some focal mechanisms on the border of the Jaz Murian depression indicate strike-slip faulting, as paleostress calculations (Figure *21*).

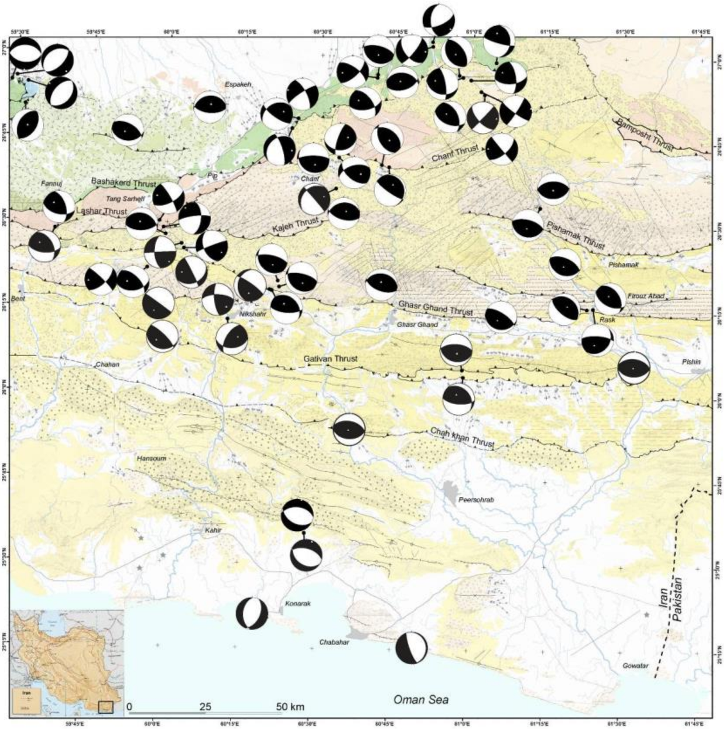

Figure 21: Focal mechanism type representation of calculation tensors of the study area. The tensor data are presented in Table 1. Compressional and extensional quadrants as in Figure 20.

Focal mechanisms in Coastal and off-shore Makran indicate compressional thrusting and strike-slip faulting, in contrast to the extension obtained from paleostress calculations (Fig. 3-80). All earthquakes related to active compression have depths >18 km (Table

2 and Table *3*). Two earthquakes related to normal faulting (Table 3-3, numbers 6 and 15) occurred at 26 and 5 km depth. These relationships indicate that extension occurs in a crustal regime while compression is deep-seated, perhaps closely related to the subducting slab (Engdahl et al. 2006; Byrne 1992, Jacob and Quittmeyer 1979). It is worth noting that the extensional focal mechanisms show radial extension like the calculated tensors in Coastal Makran (Figure *20* and Figure *21*).

Conclusion

The calculation of paleostress tensors is an important structural tool if the relationships to the regional tectonics are defined. This study is the first paleostress analysis in MAW. It shows that the regionally distributed and dominant compressional to tranpressional regimes are consistent with the orientation of folds, thrusts and strike-slip faults in all lithologies, from the Cretaceous to the Upper Miocene. NNE–SSW compression is also consistent with the active stress field obtained from focal mechanisms. We conclude that the structural development of MAW evolved under a quite stable stress field, with a compression direction coherent with the direction of convergence between the Arabian and Iranian plates (e.g. Vernant et al. 2004).

Extension characterizes a more complex and timelier less stable system. Coastal Makran seems to register regional, radial extension. Our field observation and seismic data from offshore Makran (e.g. Ellouz et. al. 2007; Grando and McClay, 2004) indicate the activity of normal faults during Pleistocene to present times. Local extensional events are recorded in the North Makran area, for example in releasing bends of strike-slip faults.

The excellent fit between calculated stress tensors and focal mechanisms data should help predicting the types of earthquakes one may have to face in the region.

Discussion and conclusions

The most recent geological maps of the study area were published in the 1970ies. They revealed to be untrustworthy because of many stratigraphic and structural misinterpretations. This study provides a new geological map and cross sections of the central onshore Makran Accretionary Wedge, in Iran. The most important results concern the stratigraphy, the tectonics and detailed structure and the evolution of the wedge through time.

Stratigraphy and structure

1- Four main structural and stratigraphic provinces are separated by major thrusts. They are, from north to south: North-, Inner, Outer and Coastal Makran.

a- North Makran comprises mainly Cretaceous sediments and volcanic rocks, in part juxtaposed within tectonic mélanges. The Lower Cretaceous (Berriasian to Barremian) sediments, mainly marl and hemipelagic limestones, were deposited in a deep-marine environment with contemporaneous volcanic activity (base of Fannuj Unit). This sedimentary environment lasted, in places, up to the Late Cretaceous (Campanian–Maastrichtian, Takht-e-Malek and Fannuj Units). However, this oceanic assemblage was locally affected by thrusting, eroded and unconformably overlain by Upper Cretaceous shallow-water limestones. During Late Cretaceous-Paleocene times, turbiditic sequences were deposited while the volcanic activity continued. Clasts of mafic to ultramafic rocks (Fannuj Unit) in the Upper Cretaceous–Paleocene sediments (Maskutan Unit) suggest erosion of ophiolites and oceanic sediments at this time. The unconformity between Upper Cretaceous shallow-water limestone and Lower Cretaceous deep-marine sediments and volcanic rocks may reflect this tectonic event.

Open and rounded folds with a very weakly spaced cleavage and the fault distribution indicate weak deformation postdating mélange formation. Folding becomes more pronounced southward, towards the N- to NE-dipping Bashakerd Thrust Zone.

b- Inner Makran, between the Bashakerd Thrust in the north and the Ghasr Ghand and Kahorkan Thrusts in the south, contains Lower Eocene to Mid Miocene successions with different sedimentary facies. The Lower Eocene deep-marine sediments and volcanic rocks grade upward into Eocene and Lower Oligocene, deeper marine turbiditic sequences, which show a general upward thickening and coarsening trend. Well preserved Nummulite faunas in turbiditic sandstones indicate shallow-water carbonate deposition north of the turbidite basin. The turbidites become more terrigenous and proximal (channelized) during the Oligocene, which suggests progradation of submarine fans (Markan and Pirdan Units), followed by the deposition of base-of slope shales and turbidites during the Late Oligocene (Rask Unit). Northeast of Rask, Upper Oligocene pro-Delta turbidites grade up-section into sandstones deposited on a shelf dominated by waves and tidal currents. During the Early Miocene, marls with gypsum (Ghasr Ghand Unit) were deposited in basins with restricted circulation. These deposits grade laterally into bioclastic sandstones and marls (Pishamak Unit). Plant remains suggest an emerged source area, somewhere to the north. The Middle Miocene sediments are turbiditic sequences, deposited in an outer fan environment. The passage between the Middle Miocene turbidites (Peersohrab Unit) and older units is not clear. Growth structures within the unit indicate deposition in a tectonically active basin.

Asymmetric, S-vergent, closed to tight folds with a well developed axial-plane cleavage in the Eocene and Oligocene turbidites of Inner Makran indicate intense shortening. In contrast, the folds in the Miocene sediments are symmetric, round and open-gentle with large wavelength (>500m) and a weak, spaced axial-plane cleavage, which suggests weaker deformation. The parallel trends of folding in Miocene and older rocks suggest a consistent compression direction during these period. The major Thrusts dip to the N. Large box folds and flat-and-ramp fault systems are evidence of large-scale décollement leading to pronounced fault-propagation folds.

c- Outer Makran, between the Ghasr Ghand Thrust in the north and the Chah Khan Thrust, to the south, consists of Lower Miocene marls with gypsum that grade laterally into bioclastic sandstones and marls (Roksha Units) and coral limestones (Vaziri Unit). Again, plant remains document an emerged area to the north. The passage from the Lower Miocene to the Middle Miocene has not been observed. The Middle Miocene starts with deep-marine turbidites that grade up-section into shallower facies.

Essentially symmetric, open to gentle, rounded folds with a large wavelength (>500m). are dominant in the Lower and Middle Miocene series with very weak, spaced axial-plane cleavage indicating a rather weak deformation in this area.

North, Inner and Outer Makran are covered unconformably by a widespread olistostrome attributed to a catastrophic event of Tortonian age. It includes blocks derived from North Makran and reworked chunks of sediments, mainly turbidites from the Inner and Outer Makran. Exotic blocks of Eocene shallow-water limestone, which were not observed in other outcrops, Cretaceous volcanic rocks, radiolarites, limestones and ophiolites, indicate derivation from the north, where ophiolite mélanges have been exposed and overlain by Eocene shallow-water limestones.

d- Coastal Makran is the lowermost tectonic unit. It includes shallow-marine sediments mostly younger than Late Miocene. The lower part of Upper Miocene successions includes fanglomerates becoming finer up-section and grading into marls. The youngest shallow marine deposits, Pliocene–Pleistocene in age (Chabahar Unit), occur only along the coast.

E–W folds are symmetric, open-gentle and rounded-blunt with very long wavelengths (>10 km) and low amplitudes. They become relatively wider and more gentle southward which reflects southward propagation of deformation. Normal faults cut sediments younger than Upper Miocene.

The calculation of paleostress tensors indicates general compressive to transpressive regimes. They are consistent with folds, thrusts and strike-slip faults in all formation, from the Cretaceous to the Upper Miocene. NNE–SSW compression is also consistent with the active stress field documented from focal mechanisms of earthquakes.

Extension characterizes a system more complex and less stable over the time. Coastal Makran seems to register regional, radial extension. Local extensional events are recorded in North Makran, for example in releasing bends of strike-slip faults.

Geochronology

Two different sets of data were obtained. Low-temperature thermochronology is documented by zircon and apatite fission track data and volcanic ash layers could be radiometrically dated by the U-Pb, SHRIMP technique.

From the apatite fission track (AFT) data and tectono-stratigraphic observations, the timing of thrust movements could be constrained. It reveals a general progression of thrusting and folding from north to south, from <23 Ma to about 7.9 Ma (Figure *22*). This is consistent with models of growing accretionary wedges (e.g. Dahlen et al., 1984). The 11.6-9.6 Ma olistostrome seals some thrust contacts and likely controlled younger out-of-sequence activity of the Ghasr Ghand Thrust. Smit et al. (2010) discussed the consequences of instantaneous deposition of a large olistostromes that triggers changes in the deformation pattern in the wedge. Their model explains how thrusts in Inner Makran become inactive or reactivated with the emplacement of the olistostrome. The emplacement of the olistostrome is probably also responsible for a southward jump of accretion to the front of the active, submarine wedge.

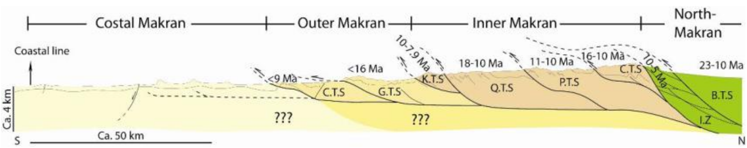

Figure 22: Schematic cross section through the onshore MAW. Timing of the activity of the individual thrusts is indicated. Abbreviations of thrust sheets: Bashakerd (BTS), Imbricate Zone (I.Z) Chanf/Lashar (C.T.S), Pishamak/Kajeh (P.T.S), Ghasr Ghand (Q.T.S), Kahorkan (K.T.S), Gativan (G.T.S) and Chah Khan (C.T.S). Vertical scale exaggerated 3x.

None of the AFT samples has undergone full annealing. This implies temperatures in the range of 60ºC–110ºC and may suggest that the presently outcropping rocks were uplifted and exhumed above a flat décollement and a blind stacking zone. The décollement would be ca. 5–6 km deep in accordance with the ca. 20ºC/km geothermal gradient of the region (Harms et al. 1984 and Khan et al. 1991). If we assume, in view of the low burial temperatures of the exhumed sediments, a relatively shallow décollement horizon, the

Upper Oligocene and Middle Miocene shales are likely candidates. The estimated depth and stratigraphic attribution suggest that important décollement levels exist within the wedge, at variance with usual wedge models that accept one major décollement at the top of the subducting slab.

Zircon fission track (ZFT) data indicate continued volcanic input into the Makran sedimentary basins from the Cretaceous through to the Eocene and to the present. The ZFT age population suggests that the Sanandaj-Sirjan Belt, to the north, is the probable source for zircon with a Cretaceous or Eocene ZFT age. The repeated occurrence of Cretaceous to Oligocene ZFT age populations in younger sediments points to recycling and reworking of the wedge sediments, especially in Miocene times. This implies surface uplift and erosion of the various thrust sheets, which then supplied the recycled sediment.

General discussion

It is generally said that the MAW has one of the lowest (2-3°) taper angles (e.g. Minshull and White 1989; Kukowski et al. 2001; Schlüter et al. 2002). In items of bulk geometry, the accretionary wedges most similar to MAW are the Southern Antilles, Burma and Andaman, which have taper angles of about 3.5º (e.g. Moore et al. 1982; Brown and Westbrook 1988; Lallemand et al. 1994; Saffer and Bekins 2006). It is argued that pore pressure strongly influences the taper angle by modifying basal and internal shear strength. On this basis, increasing sediment thickness in the trench and decreasing permeability of the sediments in the wedge would, together, lead increased pore pressure in the wedge and thus to a lower taper angle. Active margins with sediment thickness of > 4000 m are characterized by small (<4º) taper angles. The 7000 m sediment thickness recorded in the MAW possibly explains its very small taper. However, an influence of the age of the oceanic lithosphere and convergence rate on the subduction angle cannot be discarded. Old, dense lithosphere readily sinks and results in relatively steep subduction zones (Mariana type), whereas subduction of young lithosphere is buoyant and characterises shallow subduction zones like in Chile (Jarrard 1986). In the Marianas, a strong extensional regime developed in the back arc basin, due to weak coupling between the two converging plates. However, in contrast to the Chilean-Andes, the subduction zone is strongly compressive. Jarrard (1986) subdivided subduction zones into seven strain classes from a strongly extensional class 1 to a strongly compressional class 7. Makran does not appear in this kinematic classification. Indeed, comparison of oceanic lithosphere ages in active margins (Muller et al. 1996) indicates that the old (100–70 Ma) oceanic lithosphere of Makran subducts at a shallower angle than the younger oceanic lithospheres of Andaman (ca. 55–47 Ma) or south Antilles (ca. 67–55Ma). This apparent paradox points to the complexity of subduction zones. In Makran, fluids entrained in the subduction zone may play an important role in allowing important sediment underplating below the mid-wedge décollements.

Outlook

Our work leaves several questions open. Future work should include:

- Detailed mapping of North Makran to better understand its tectonic evolution and the structural relationship of MAW with Jaz Murian as a potential backstop zone.

- Investigations as to whether the Imbricate Zone in the north of Fannuj and that East of Espakeh belong to the same or different units.

- Heavy mineral and paleocurrent analyses in the clastic successions in order to specify the source areas.

- Detailed measurements of sections and definition of the facies evolution in the turbiditic sequences in order to understand the dynamics and the tectonic evolution of the sedimentary basins.

- Defining the stratigraphic boundaries between Eocene and Oligocene, Lower Miocene and Middle Miocene formations.

- Understanding the extension in North and in Coastal Makran.

References:

Alinaghi, A. Koulakov, I. and Thybo, H. 2007. Seismic tomographic imaging of P- and S-waves velocity perturbations in the upper mantle beneath Iran. Geophys. J. Int. 169: 1089-1102.

Anderson, E.M., 1905. The dynamics of faulting. Transactions of the Edinburgh Geological Society, 8(3), pp.387-402.

Angelier, J. (1984). Tectonic analysis of fault slip data sets. Journal of Geophysical Research 89(B7): 5835- 5848.

Armijo, R., Carey, E. and Cisternas, A., 1982. The inverse problem in microtectonics and the separation of tectonic phases. Tectonophysics, 82(1-2), pp.145-160.

Arthurton, R. S. Farah, A. Wahiduddin, A. (1982). The Late Cretaceous-Cenozoic history of western

Berberian, F. Muir, I. D. Pankhurst, R. J. Berberian, M.1982. Late Cretaceous and early Miocene Andean-type plutonic activity in northern Makran and central Iran. Journal of the Geological Society of London 139 Part 5: 605-614.

Bijwaard, H. Spakman, W. Engdahl, E.R. 1998. Closing the gap between regional and global travel time tomography. Journal of Geophysical Research 103(B 12): 55-78.

Bird, P. Toksoz, M.N. Sleep, N.H. 1975. Thermal and mechanical models of continental-continental convergence zones. Geophysical research letters 80: 4405-4416.

Bott, M. H. P. (1959). The mechanics of oblique slip faulting. Geological Magazine 96 109–117.

Brown, K. and Westbrook, G. K. 1988. Mud diapirism and subcretion in the Barbados ridge accretionary complex: the role of fluids in accretionary processes. Tectonics 7(3): 613-640.

Burg, J.-P. Célérier, B. Chaudhry, N. M.; Ghazanfar, M. Gnehm, F.; Schnellmann, M. 2005. Fault analysis and paleostress evolution in large strain regions: methodological and geological discussion of the southeastern Himalayan fold-and-thrust belt in Pakistan. Journal of Asian Earth Sciences 24(4): 445-467.

Byrne, D. E. Sykes, L.R. Davis, D.M. 1992. Great Thrust Earthquakes and aseismic Slip Along the Plate Boundary of the Makran Subduction Zone. Geophysical research 97(No. B1): 449-478.

Célérier, B. 1988. How much does slip on a reactivated fault plane constrain the stress tensor? Tectonics 7(6): 1257-1278.

Célérier, B., 1995. Tectonic regime and slip orientation of reactivated faults. Geophysical Journal International, 121(1), pp.143-161.

Célérier, B. (1999). Fault slip analysis software. http://www.isteem.univmontp2.fr/PERSO/celerier/software/software.bc.html.

Chandra, U. 1984. Focal mechanism solutions for earthquakes in Iran. Physics of the Earth and Planetary Interiors 34(1-2): 9-16.

Cowie, P.A. and Scholz, C.H., 1992. Physical explanation for the displacement-length relationship of faults using a post-yield fracture mechanics model. Journal of Structural Geology, 14(10), pp.1133-1148.

Dahlen, F. A. Suppe, J. Davis, D. 1984. Mechanics of fold-and-thrust belts and accretionary wedges: Cohesive Coulomb theory. Journal of geophysical research 89(B12): 87-101.

Dercourt, J. Zonenshain, L. P. Ricou, L. E. Kazmin, V. G. Le Pichon, X. Knipper, A. L. Grandjacquet, C. Sbortshikov, I. M. Geyssant, J. Lepvrier, C. Pechersky, D. H. Boulin, J. Sibuet, J.

C. Savostin, L. A. Sorokhtin, O. Westphal, M. Bazhenov, M. L. Lauer, J. P. Biju-Duval, B. 1986. Geological evolution of the Tethys belt from the Atlantic to the Pamir since the LIAS. Tectonophysics 123(1-4): 241-315.

Dolati, A., 2010. Stratigraphy, structural geology and low-temperature thermochronology across the Makran accretionary wedge in Iran (Doctoral dissertation, ETH Zurich).

Dupin, J.-M. Sassi, W. Angelier, J. (1993). Homogeneous stress hypothesis and actual fault slip: a distinct element analysis. Journal of Structural Geology 18(8): 1033-1043.

Ellouz-Zimmermann, N. Deville, E. Müller, C. Lallemant, S. Subhani, A.B. Tabreez, A.R. 2007. Impact of sedimentation on convergent margin tectonics: Example of the Makran accretionary prism (Pakistan). Thrust belts and foreland basins from fold kinematics to hydrocarbon systems. O. L. Lacombe, J.; Roure, F.; Verges, J. Springer: 326-348.

Ellouz-Zimmermann, N. Lallemant, S.J. Castilla, R. Mouchot, N. Leturmy, P. Battani, A. Buret, C. Cherel, L. Desaubliaux, G. Deville, E. Ferrand, J. Lügcke, A. Mahieux, G. and G. Mascle, Mühr, P. PiersonWickmann, A.-C. Robion, P. Schmitz, J. Danish, M. Hasany, S. Shahzad, A. Tabreez, A. (2007). Offshore frontal part of the Makran accretionary prism (Pakistan) The Chamak Survey. Thrust belts and foreland
basins from fold kinematics to hydrocarbon systems. O. L. Lacombe, J.; Roure, F.; Verges, J. Springer: 349-364.

Engdahl, E. R. Jackson, J. A. Myers, S. C. Bergman, E. A. and Priestley, K. 2006. Relocation and assessment of seismicity in the Iran region. Geophys. J. Int. 167: 761-778.

Etchecopar, A. and Malavieille, J., 1987. Computer models of pressure shadows: a method for strain measurement and shear-sense determination. Journal of structural Geology, 9(5-6), pp.667-677.

Farhoudi, G. and Karig, D. E. 1977. Makran of Iran and Pakistan as an active arc system. Geology 5(11): 664- 668.

Frohlich, C., 1992. Triangle diagrams: ternary graphs to display similarity and diversity of earthquake focal mechanisms. Physics of the Earth and Planetary interiors, 75(1-3), pp.193-198.

Fruehn, J. Reston, T. von Huene, R. Bialas, J. 2002. Structure of the Mediterranean Ridge accretionary complex from seismic velocity information. Marine Geology 186 (1-2): 43-58.

Grando, G. and McClay, K., 2004. Structural evolution of the Frampton growth fold system, Atwater Valley-Southern Green Canyon area, deep water Gulf of Mexico. Marine and Petroleum Geology, 21(7), pp.889-910.

Grando, G. and McClay, K. 2006. Morphotectonics domains and structural styles in the Makran accretionary prism, offshore Iran. Sedimentary Geology 196(1-4): 157-179.

Grando, G. and McClay, K., 2007. Morphotectonics domains and structural styles in the Makran accretionary prism, offshore Iran. Sedimentary geology, 196(1-4), pp.157-179.

Hafkenscheid, E. Wortel, M. J. R. and Spakman, W. 2006. Subduction history of the Tethyan region derived from seismic tomography and tectonic reconstructions. J. Geophys. Res. 111(B08401): doi:10.1029/2005JB003791.

Harms, J. C. Cappel, H. N. Francis, D. C. 1984. The Makran coast of Pakistan; its stratigraphy and hydrocarbon potential. Marine geology and oceanography of Arabian Sea and coastal

Pakistan. U. Haq Bilal, Milliman John, D. New York, NY, United States, Van Nostrand Reinhold Co.: 3-26.

Hutchison, I. Louden, K.E. White, R.S. 1981. Heat flow and age of the Gulf of Oman. Earth and Planetary Science Letters, 56: 252-262.

Jackson, J. Mckenzie, D. (1984). Active tectonics of the Alpine–Himalayan Belt between western Turkey and Pakistan. Geophysical Journal of the Royal Astronomical Society 77(1): 185-264.

Jacob, K. H. and Quittmeyer R. L. 1979. The Makran region of Pakistan and Iran: Trench-arc system with active plate subduction. Geodynamics of Pakistan. A. Farah and K. A. de Jong. Quetta, Pakistan: 305-317.

Jarrard, R. D. 1986. Relations among subduction pattern. Reviews of Geophysics 24: 217-284.

Khan, M. A. Raza, H. A. Alam, S. 1991. Petroleum geology of the Makran region; implications for hydrocarbon occurrence in cool basins. Journal of Petroleum Geology 14(1): 5-18.

Kopp, C. Fruehn, J. Flueh, E. R. Reichert, C. Kukowski, N. Bialas, J. Klaeschen, D. 2000. Structure of the Makran subduction zone from wide-angle and reflection seismic data. Deep seismic profiling of the continents and their margins. R. Carbonell, Gallart, J. Torne, M. Elsevier. Amsterdam, Netherlands. 2000.

Kukowski, N. Lallemand, S. E. Malavieille, J. Gutscher, M-A. Reston, T. J. 2002. Mechanical decoupling and basal duplex formation observed in sandbox experiments with application to the Western Mediterranean Ridge accretionary complex. Marine Geology 186(1-2): 29-42.

Kukowski, N. Schillhorn, T. Huhn, K. Von Rad, U. Husen, S. Flueh, E. 2001. Morphotectonics and mechanics of the central

Makran accretionary wedge off Pakistan. Marine Geology 173(1-4): 1-19.

Laane, J. L. and Chen, W. P. 1989. The Makran earthquake of 1983 April 18; a possible analogue to the Puget Sound earthquake of 1965? Geophysical Journal of the Royal Astronomical Society 98(1): 1-9.

Lallemand, S. E. Schnürle, P. Malavieille, J. 1994. Coulomb theory applied to accretionary and nonaccretionary wedges: Possible causes for tectonic erosion and/or frontal accretion. J. Geophys. Res. 99(B6): 12033-12055.

McCall, G. J. H. 1983. Mélange of the Makran, Southeastern Iran. Benchmark papers in Geology 66: 292-299.

McCall, G. J. H. and Kidd R. G. W. 1982. The Makran, southeastern Iran; the anatomy of a convergent plate margin active from Cretaceous to present. Trench-Forearc geology; sedimentation and tectonics on modern and ancient active plate margins, conference. K. Leggett Jeremy. London, United Kingdom, Geological Society of London. 10: 387-397.

Minshull, T. A. White, R. S. Barton, P. J. Collier, J. S. 1992. Deformation at plate boundaries around the gulf of Oman. Marine Geology 104(1-4): 265-277.

Molnar, P. Stock, J. M. (2009). Slowing of India's convergence with Eurasia since 20 Ma and its implications for Tibetan mantle dynamics. Tectonics 28.

Moore, G. F. Curray J. R. and Emmel F. J. 1982. Sedimentation in the Sunda Trench and forearc region. Geological Society, London 10: 245-258.

Nilforoushan, F., Masson, F., Vernant, P., Vigny, C., Martinod, J., Abbassi, M., Nankali, H., Hatzfeld, D., Bayer, R., Tavakoli, F. and Ashtiani, A., 2003. GPS network monitors the Arabia-

Eurasia collision deformation in Iran. Journal of Geodesy, 77, pp.411-422.

Page, W. D. Alt, J. N. Cluff, L.S. Plafker, G. (1979). Evidence for the recurrence of large-magnitude earthquakes along the Makran coast of Iran and Pakistan. Recent crustal movements, 1977. C. A. Whitten, Green, R. Meade, B. K. Amsterdam, Netherlands, Elsevier. 52; 1-4: 533-547.

Paul, J. Bürgmann, R. Gaur, V. K. Bilham, R. Larson, K. M. Ananda, M. B. Jade, M. Anupama, T.S. Satyal, G. Kumar, D. 2001. The motion and active deformation of India. Geophysical Research Letters 28: 647-651.

Petit, J. P. 1987. Criteria for the sense of movement on fault surfaces in brittle rocks. Journal of structural Geology 9(5-6): 597-608.

Philip, H., 1987. Plio-Quaternary evolution of the stress field in Mediterranean zones of subduction and collision. In Annales geophysicae. Series B. Terrestrial and planetary physics (Vol. 5, No. 2, pp. 301-319).

Platt, T. and Sathyendranath, S., 1988. Oceanic primary production: estimation by remote sensing at local and regional scales. Science, 241(4873), pp.1613-1620.

Quittmeyer, R. C. Kafka, A. L. Armbruster, J.C. 1984. Focal mechanisms and depths of earthquakes in central Pakistan; a tectonic interpretation. Journal of Geophysical Research 89: 2459-2470.

Reilinger, R. McClusky, S. Vernant, P. Lawrence, S. Ergintav, S. Cakmak, R. Ozener, H. Kadirov, F. Guliev, I. Stepanyan, R. Nadariya, M. Hahubia, G. Mahmoud, S. K. ArRajehi, A. Paradissis, D. Al-Aydrus, A. Prilepin, M. Guseva, T. Evren, E. Dmitrotsa, A. Filikov, S. V. Gomez, F. Al-Ghazzi, R. Karam, G. (2006). GPS constraints on continental deformation in the Africa-Arabia-Eurasia continental collision zone and implications for the dynamics of plate interactions. J. Geophys. Res. 111(B05411): doi:10.1029/2005JB004051.

Saffer, D. M. and Bekins, B. A. 2006. An evaluation of factors influencing pore pressure in accretionary complexes: Implications for taper angle and wedge mechanics. Journal of Geophysical Research-Solid Earth 111(B4).

Schlüter, H.U., Prexl, A., Gaedicke, C., Roeser, H., Reichert, C., Meyer, H. and Von Daniels, C., 2002. The Makran accretionary wedge: sediment thicknesses and ages and the origin of mud volcanoes. Marine Geology, 185(3-4), pp.219-232.

Schott, B. and Koyi, H. A. 2001. Estimating basal friction in accretionary wedges from the geometry and spacing of frontal faults. Earth and Planetary Science Letters 194(1-2): 221-227.

Smit, J., Burg, J.P., Dolati, A. and Sokoutis, D., 2010. Effects of mass waste events on thrust wedges: Analogue experiments and application to the Makran accretionary wedge. Tectonics, 29(3).

Stöcklin, J. 1968. Structural history and tectonics of Iran, a review. Assoc. Petrol. Geol. Bull. 52(1220-1258).

Stoneley, R. 1974. Evolution of the continental margins bounding a former southern Tethys. the geology of Continental margins: 889-903.

Vernant, P. h. Nilforoushan, F. Hatzfeld, D. Abbassi, M. R. Vigny, C. Masson, F. Nankali, H. Martinod, J. Ashtiani, A. Bayer, R. Tavakoli, F. Chery, J. 2004. Present-day crustal deformation and plate kinematics in the Middle East constrained by GPS measurements in Iran and northern Oman. Geophysical Journal International 157(1): 381-398.

Wallace, A. F. C. (1956). Revitalization Movements. American Anthropologist 58(2): 264-281.

Westbrook, G. K. Ladd, J. W. Buhl, P. Bangs, N. Tiley, G. J. 1988. Cross section of an accretionary wedge: Barbados Ridge complex. Geology 16(7): 631-635.

White, R. S. Klitgord, K. 1976. Sediment deformation and plate tectonics 1n the Gulf of Oman. Earth and Planetary Science Letters 32.

White, R. S. and Louden, K. E. 1982. The Makran continental margin; structure of a thickly sedimented convergent plate boundary. Studies in continental margin geology. S. Watkins Joel and L. Drake Charles. Tulsa, OK, United States, American Association of Petroleum Geologists. 34: 499-518.